

DFTT 30/95  
 JHU-TIPAC 95017  
 hep-ph/9505301

# ATMOSPHERIC NEUTRINO OSCILLATIONS AMONG THREE NEUTRINO FLAVORS AND LONG-BASELINE EXPERIMENTS

S.M. Bilenky<sup>a,b</sup>, C. Giunti<sup>a</sup> and C. W. Kim<sup>c</sup>

<sup>a</sup>*INFN, Sezione di Torino and Dipartimento di Fisica Teorica, Università di Torino,  
 Via P. Giuria 1, 10125 Torino, Italy*

<sup>b</sup>*Joint Institute of Nuclear Research, Dubna, Russia*

<sup>c</sup>*Department of Physics and Astronomy, The Johns Hopkins University,  
 Baltimore, Maryland 21218, USA.*

(July 2, 2021)

## Abstract

Anticipating future long-baseline neutrino experiments to search for neutrino oscillations in various oscillation channels, we have analyzed the atmospheric neutrino data in the framework of a model with mixing of three massive neutrino fields that can accommodate the data of solar neutrino experiments. The oscillations of atmospheric and terrestrial neutrinos are described in this model by three parameters:  $\Delta m^2$  and the squared moduli of two elements of the mixing matrix,  $|U_{e3}|^2$  and  $|U_{\mu 3}|^2$ , which determine the amplitudes of oscillations among all active neutrinos. The results of the analysis of the atmospheric neutrino data are presented in the form of allowed regions in the plane of the two parameters oscillation amplitude and  $\Delta m^2$  for all oscillation channels to be investigated in the future long-baseline oscillation experiments.

## I. INTRODUCTION

The question of neutrino mass and mixing is the central issue in modern neutrino physics. The search for the effects of neutrino mass and mixing and the investigation of the nature of massive neutrinos (Dirac or Majorana?) may provide an important clue to explore and understand the physics beyond the standard model.

Important indications in favor of neutrino mixing have emerged from the solar neutrino data. In all four solar neutrino experiments [1–4], that are sensitive to different parts of the solar neutrino spectrum, the observed event rates are significantly less than the event rates predicted by the standard solar model. All the existing solar neutrino data can be described with the assumption that neutrinos are mixed and the resonant MSW mechanism takes place in the Sun [5]. For the two parameters  $\Delta m^2$  and  $\sin^2 2\vartheta$  ( $\Delta m^2 \equiv m_2^2 - m_1^2$ ,  $m_1$  and  $m_2$  being the neutrino masses, and  $\vartheta$  the mixing angle) the following values were obtained:

$$\Delta m^2 \simeq 5 \times 10^{-6} \text{ eV}^2 \quad \text{and} \quad \sin^2 2\vartheta \simeq 8 \times 10^{-3} \quad (\text{small mixing angle solution}) , \quad (1.1)$$

$$\Delta m^2 \simeq 10^{-5} \text{ eV}^2 \quad \text{and} \quad \sin^2 2\vartheta \simeq 0.8 \quad (\text{large mixing angle solution}) . \quad (1.2)$$

Other indications in favor of neutrino mixing come from the so called atmospheric neutrino anomaly. The flux ratio of the atmospheric  $\nu_\mu$  and  $\nu_e$  is close to 2 and is predicted with accuracy better than 5% [6–9]. For the ratio of ratios

$$R \equiv \frac{N_\mu^{\text{exp}}/N_e^{\text{exp}}}{N_\mu^{\text{MC}}/N_e^{\text{MC}}} , \quad (1.3)$$

the Kamiokande collaboration [10–12] found the following value:

$$R = 0.60^{+0.06}_{-0.05} \pm 0.05 . \quad (1.4)$$

Here,  $N_e^{\text{exp}}$  and  $N_\mu^{\text{exp}}$  are, respectively, the number of observed  $e$ -like and  $\mu$ -like events and  $N_e^{\text{MC}}$  and  $N_\mu^{\text{MC}}$  are, respectively, the number of  $e$ -like and  $\mu$ -like events predicted by MC simulations, after passing through the same analysis chain as the data under the assumption that there are no neutrino oscillations.

The atmospheric neutrino anomaly has also been found by the IMB [13] and Soudan 2 [14] experiments. In these experiments the following values of the ratio  $R$  have been obtained:

$$R = 0.54 \pm 0.05 \pm 0.12 \quad (\text{IMB}) , \quad (1.5)$$

$$R = 0.64 \pm 0.17 \pm 0.09 \quad (\text{Soudan 2}) . \quad (1.6)$$

On the other hand, no indications in favor of the anomaly were obtained in the Frejus [15–17] and NUSEX [18] experiments. In these experiments the following values for the ratio  $R$  have been obtained:

$$R = 0.99 \pm 0.13 \pm 0.08 \quad (\text{Frejus}) , \quad (1.7)$$

$$R = 1.04 \pm 0.25 \quad (\text{NUSEX}) . \quad (1.8)$$

We also note that no indications in favor of a deficit of muon neutrinos were found in the experiments on the detection of upgoing muons. For the ratio  $r$  of the number of observed  $\mu$ -like events to the expected number of events (which is much more model dependent than the ratio of ratios  $R$ ) the following values were obtained [19–22]:

$$r = 1.03 \pm 0.04 \quad (\text{IMB}) , \quad (1.9)$$

$$r = 0.94 \pm 0.06 \quad (\text{Kamiokande}) , \quad (1.10)$$

$$r = 1.13 \quad (\text{Baksan}) , \quad (1.11)$$

$$r = 0.73 \pm 0.16 \quad (\text{MACRO}) . \quad (1.12)$$

The Kamiokande, IMB and Soudan 2 data can be explained by neutrino oscillations. From the analysis of the Kamiokande data in the simplest case of oscillations between two types of neutrinos the following allowed ranges of the parameters  $\Delta m^2$  and  $\sin^2 2\vartheta$  ( $\vartheta$  is the mixing angle) have been found [12]:

$$5 \times 10^{-3} \leq \Delta m^2 \leq 3 \times 10^{-2} \text{ eV}^2 \quad 0.7 \leq \sin^2 2\vartheta \leq 1 \quad (1.13)$$

in the case of  $\nu_\mu \rightleftharpoons \nu_\tau$  oscillations and

$$7 \times 10^{-3} \leq \Delta m^2 \leq 8 \times 10^{-2} \text{ eV}^2 \quad 0.6 \leq \sin^2 2\vartheta \leq 1 \quad (1.14)$$

in the case of  $\nu_\mu \rightleftharpoons \nu_e$  oscillations.

It is very important to note that the indications in favor of neutrino mixing coming from the atmospheric neutrino data can be checked in future experiments with terrestrial neutrinos. At present a wide range of long-baseline experiments with neutrinos from reactors and accelerators aimed to investigate neutrino oscillations in the range  $\Delta m^2 \simeq 10^{-3} - 10^{-2} \text{ eV}^2$  is under development (see Ref. [23]). In these experiments, different neutrino transitions will be investigated such as  $\bar{\nu}_e \rightarrow \bar{\nu}_e$  with reactors [24] and  $\nu_\mu \rightarrow \nu_\mu$ ,  $\nu_\mu \rightarrow \nu_e$ ,  $\nu_\mu \rightarrow \nu_\tau$  with accelerators [25–28]. In the accelerator experiments, neutral-current processes will also be investigated.

In order to accommodate the solar neutrino data and the atmospheric neutrino anomaly, corresponding to different scales for the neutrino mass squared difference, one must assume that the flavor neutrino fields are combinations of at least three fields of massive neutrinos. We will analyze here the atmospheric neutrino data in the framework of a minimal scheme with three massive neutrinos (see also Ref. [29]). In this scheme the oscillations of atmospheric and terrestrial neutrinos are characterized by three parameters,  $\Delta m^2 \equiv m_3^2 - m_1^2$  ( $\nu_3$  is the heaviest neutrino) and the squared moduli of two elements of the mixing matrix,  $|U_{e3}|^2$  and  $|U_{\mu 3}|^2$ .

We have found that the atmospheric neutrinos data are well described by this model. In presenting the results of our analysis, we have taken into account the constraints that follow from reactor and accelerator experiments which have searched for neutrino oscillations. We have obtained the allowed regions of the oscillation parameters for different oscillation channels that will be investigated in future neutrino long-baseline experiments. The results of our analysis are presented in the form convenient for a direct comparison with the data of these experiments.

In Section II we describe briefly the model under consideration. In Section III and Section IV we present the method and the results of the analysis, respectively.

## II. A MODEL WITH MIXING OF THREE MASSIVE NEUTRINO FIELDS

We assume that the fields of flavor neutrinos  $\nu_{\alpha L}$  (with  $\alpha = e, \mu, \tau$ ) are superpositions of the left-handed components of massive neutrino fields given by

$$\nu_{\alpha L} = \sum_k U_{\alpha k} \nu_{k L} \quad (\alpha = e, \mu, \tau) , \quad (2.1)$$

where  $\nu_k$  is the field of a neutrino (Dirac or Majorana) with mass  $m_k$  and  $U$  is a unitary mixing matrix.

The number of massive fields in Eq.(2.1) can range from three to six. It is to be emphasized that in most models this number is equal to three. Such mixing can take place if the neutrino masses are generated by the see-saw mechanism [30], or the neutrino mass term contains only the left-handed components of the neutrino flavor fields, or the total lepton number is conserved (see, for example, Refs. [31,32]).

In the following we assume that the number of massive fields in Eq.(2.1) is *three*. We enumerate the three neutrino masses in such a way that  $m_1 < m_2 < m_3$ . The modulus of the amplitude of  $\nu_\alpha \rightarrow \nu_\beta$  transitions in vacuum can be written in the form

$$|\mathcal{A}_{\nu_\alpha \rightarrow \nu_\beta}| = \left| \sum_{k=2}^3 U_{\beta k} \left[ \exp \left( -i \frac{\Delta m_{k1}^2 L}{2p} \right) - 1 \right] U_{\alpha k}^* + \delta_{\beta\alpha} \right| . \quad (2.2)$$

Here  $L$  is the distance between the neutrino source and detector,  $p$  is the neutrino momentum and  $\Delta m_{k1}^2 \equiv m_k^2 - m_1^2$ .

In order to describe the solar neutrino data and the atmospheric neutrino anomaly, it is necessary to assume that

$$\Delta m_{21}^2 \ll \Delta m_{31}^2 . \quad (2.3)$$

This inequality is in agreement with the assumption of a natural hierarchy of neutrino masses, which is analogous to the mass hierarchy of quarks.

From Eqs.(2.2) and (2.3) we obtain the following expression for the probability of  $\nu_\alpha \rightarrow \nu_\beta$  ( $\bar{\nu}_\alpha \rightarrow \bar{\nu}_\beta$ ) transitions (with  $\beta \neq \alpha$ ) of atmospheric and terrestrial neutrinos [33]:

$$P_{\nu_\alpha \rightarrow \nu_\beta} = P_{\bar{\nu}_\alpha \rightarrow \bar{\nu}_\beta} = \frac{1}{2} A_{\nu_\alpha; \nu_\beta} \left( 1 - \cos \frac{\Delta m^2 L}{2p} \right) . \quad (2.4)$$

Here  $\Delta m^2 \equiv \Delta m_{31}^2$  and

$$A_{\nu_\alpha; \nu_\beta} = A_{\nu_\beta; \nu_\alpha} = 4 |U_{\alpha 3}|^2 |U_{\beta 3}|^2 \quad (2.5)$$

is the amplitude of  $\nu_\alpha \leftrightarrows \nu_\beta$  ( $\bar{\nu}_\alpha \leftrightarrows \bar{\nu}_\beta$ ) oscillations.

From Eq.(2.4) we obtain the following expression for the survival probability of  $\nu_\alpha$  ( $\bar{\nu}_\alpha$ ):

$$P_{\nu_\alpha \rightarrow \nu_\alpha} = P_{\bar{\nu}_\alpha \rightarrow \bar{\nu}_\alpha} = 1 - \sum_{\beta \neq \alpha} P_{\nu_\alpha \rightarrow \nu_\beta} = 1 - \frac{1}{2} B_{\nu_\alpha; \nu_\alpha} \left( 1 - \cos \frac{\Delta m^2 L}{2p} \right) , \quad (2.6)$$

where the oscillation amplitude  $B_{\nu_\alpha;\nu_\alpha}$  is given by

$$B_{\nu_\alpha;\nu_\alpha} = \sum_{\beta \neq \alpha} A_{\nu_\alpha;\nu_\beta} . \quad (2.7)$$

From unitarity of the mixing matrix we have

$$B_{\nu_\alpha;\nu_\alpha} = 4 |U_{\alpha 3}|^2 (1 - |U_{\alpha 3}|^2) . \quad (2.8)$$

In the model under consideration there are 3 free parameters,  $\Delta m^2$ ,  $|U_{e3}|^2$  and  $|U_{\mu 3}|^2$ . From the unitarity of the mixing matrix we have  $|U_{\tau 3}|^2 = 1 - |U_{e3}|^2 - |U_{\mu 3}|^2$ . We will use the expressions in Eqs.(2.4) and (2.6) for the analysis of atmospheric neutrino data and for the discussion of future long-baseline experiments.

In the model under consideration all oscillation channels are open and the probabilities of all possible transitions of atmospheric and terrestrial neutrinos have the same form as in the case of oscillations between two neutrino types. This is related to the fact that all the expressions of the transition probabilities depend only on one neutrino mass squared difference and the oscillation length  $L_{\text{osc}} = 4\pi p/\Delta m^2$  is the same for all channels. However, each oscillation channel is characterized by its own amplitude. The oscillation amplitudes are related by (see Eq.(2.7))

$$A_{\nu_\mu;\nu_e} + A_{\nu_\mu;\nu_\tau} = B_{\nu_\mu;\nu_\mu} , \quad (2.9)$$

$$A_{\nu_\mu;\nu_e} + A_{\nu_e;\nu_\tau} = B_{\nu_e;\nu_e} . \quad (2.10)$$

We add here that the oscillation amplitudes  $A_{\nu_\alpha;\nu_\beta}$  satisfy the following relation:

$$\left( \frac{A_{\nu_\mu;\nu_e} A_{\nu_\mu;\nu_\tau}}{A_{\nu_e;\nu_\tau}} \right)^{1/2} + \left( \frac{A_{\nu_\mu;\nu_e} A_{\nu_e;\nu_\tau}}{A_{\nu_\mu;\nu_\tau}} \right)^{1/2} + \left( \frac{A_{\nu_e;\nu_\tau} A_{\nu_\mu;\nu_\tau}}{A_{\nu_\mu;\nu_e}} \right)^{1/2} = 2 . \quad (2.11)$$

This relation follows from Eq.(2.5) and the unitarity of the mixing matrix.

### III. THE METHOD OF ANALYSIS OF THE DATA

In this section we describe our method of analysis of the experimental data. As a first step we have analyzed only the Kamiokande data. Then, we have carried out a combined analysis of the Kamiokande and Frejus data.

The Kamiokande collaboration has measured the ratio of ratios  $R$  in two ranges of energies: the sub-GeV range with energies of contained events less than 1.33 GeV and the multi-GeV range with energies of contained and partially contained events more than 1.33 GeV. The measured values of the ratio  $R$  in these two regions agree with each other:

$$R = 0.60^{+0.06}_{-0.05} \pm 0.05 \quad (\text{sub-GeV energy range}) , \quad (3.1)$$

$$R = 0.57^{+0.08}_{-0.07} \pm 0.07 \quad (\text{multi-GeV energy range}) . \quad (3.2)$$

The Kamiokande collaboration has also investigated the dependence of the ratio  $R$  on the zenith-angle  $\theta$  ( $\theta = 0$  corresponds to downward-going neutrinos). Some indications in favor of a zenith-angle dependence of the ratio  $R$  were found in the multi-GeV region.

The experimental data are divided into 5 bins corresponding to the following averaged values of  $\cos \theta$ :  $\langle \cos \theta \rangle_{i=1,\dots,5} = -0.8, -0.4, 0.0, 0.4, 0.8$  and the averaged distances  $\langle L \rangle_{i=1,\dots,5} = 10, 230, 5, 157, 852, 54, 26$  Km, respectively. The number  $N_e^i$  of  $e$ -like events and the number  $N_\mu^i$  of  $\mu$ -like events in the bin  $i$  are given by

$$N_e^i = N_e^{i\text{MC}} P_{\nu_e \rightarrow \nu_e}^i + N_\mu^{i\text{MC}} P_{\nu_\mu \rightarrow \nu_e}^i, \quad (3.3)$$

$$N_\mu^i = N_e^{i\text{MC}} P_{\nu_e \rightarrow \nu_\mu}^i + N_\mu^{i\text{MC}} P_{\nu_\mu \rightarrow \nu_\mu}^i. \quad (3.4)$$

Here  $N_e^{i\text{MC}}$  and  $N_\mu^{i\text{MC}}$  are, respectively, the number of  $e$ -like and  $\mu$ -like events predicted by MC simulations under the assumption that there are no oscillations and  $P_{\nu_\alpha \rightarrow \nu_\beta}^i$  is the averaged probability of  $\nu_\alpha \rightarrow \nu_\beta$  transitions (with  $\alpha, \beta = e, \mu$ ). From Eqs.(3.3) and (3.4), we obtain the ratio of the ratios  $R_i$  in the bin  $i$

$$R_i = \frac{P_{\nu_\mu \rightarrow \nu_\mu}^i + (N_\mu^{i\text{MC}}/N_e^{i\text{MC}})^{-1} P_{\nu_e \rightarrow \nu_\mu}^i}{P_{\nu_e \rightarrow \nu_e}^i + (N_\mu^{i\text{MC}}/N_e^{i\text{MC}}) P_{\nu_\mu \rightarrow \nu_e}^i}. \quad (3.5)$$

In our calculation we take into account 30% errors of the MC calculations of the total number of  $e$ -like and  $\mu$ -like events due to the fact that different calculations give different neutrino fluxes. The errors of the MC calculations of the  $\mu/e$  ratio are much smaller: 9% for the Kamiokande sub-GeV data, 12% for the Kamiokande multi-GeV data and 14% for the Frejus data. In our calculations we have neglected the fact that not all  $e$ -like and  $\mu$ -like events are produced by  $\nu_e$  ( $\bar{\nu}_e$ ) and  $\nu_\mu$  ( $\bar{\nu}_\mu$ ) interactions, respectively. The purity of the  $e$ -like and  $\mu$ -like events is estimated by the Kamiokande Collaboration to be higher than 90%.

For the fit of the sub-GeV Kamiokande data we have used the ratio of ratios given in Eq.(3.5). For the fit of the multi-GeV Kamiokande data and the Frejus data we have used the number of  $e$ -like and  $\mu$ -like events given in Eqs.(3.3) and (3.4). The expected numbers of  $e$ -like and  $\mu$ -like events,  $N_e^{i\text{MC}}$  and  $N_\mu^{i\text{MC}}$ , were taken from Fig.2 of Ref. [10] for the Kamiokande sub-GeV data, from Fig.3 of Ref. [12] for the Kamiokande multi-GeV data and from Fig.4 of Ref. [15] for the Frejus data, respectively. The quantities  $P_{\nu_e \rightarrow \nu_\mu}^i$  and  $P_{\nu_\mu \rightarrow \nu_e}^i$  are the  $\nu_e \rightarrow \nu_\mu$  and  $\nu_\mu \rightarrow \nu_e$  transition probabilities averaged over the neutrino energy spectrum and the zenith-angles of bin  $i$ . These probabilities depend on the value of  $\Delta m^2$  and they are different because the initial  $\nu_e$  and  $\nu_\mu$  have different energy spectra. These energy spectra are given in Fig.1 of Ref. [11] for the Kamiokande sub-GeV region, in Fig.2 of Ref. [12] for the Kamiokande multi-GeV region and in Fig.3 of Ref. [15] for the Frejus experiment, respectively.

Since the expressions (2.4) and (2.6) that we use for the transition and survival probabilities of flavor neutrinos are valid in vacuum, we do not consider in our analysis the Kamiokande multi-GeV data on upward-going neutrinos, for which the matter effect could be important (see Ref. [34]).

Finally, we would like to emphasize that our analyses take into account the possibility of simultaneous oscillations among all three neutrino types:  $\nu_\mu \rightleftharpoons \nu_e$ ,  $\nu_\mu \rightleftharpoons \nu_\tau$  and  $\nu_e \rightleftharpoons \nu_\tau$ . This analysis is quite different from the usual two generation analyses, where the two oscillation channels  $\nu_\mu \rightleftharpoons \nu_e$  and  $\nu_\mu \rightleftharpoons \nu_\tau$  are considered separately, leading to two possible unrelated interpretations of the data.

#### IV. RESULTS OF THE ANALYSIS

The results of the analysis of the Kamiokande data in the framework of the model with oscillations among three neutrino flavors discussed in Section II are presented in Figs.1–4. We have obtained a rather good description of the data, i.e. for 8 degrees of freedom we obtained  $\chi^2_{\min} = 3.2$  at  $\Delta m^2 = 2.7 \times 10^{-2} \text{ eV}^2$ ,  $|U_{e3}|^2 = 0.14$  and  $|U_{\mu 3}|^2 = 0.62$  (with a confidence level (CL) of 92%). In the figures we present the results of our analysis in terms of two-parameter allowed regions at 90% CL (these regions are given by  $\chi^2 \leq \chi^2_{\min} + 4.6$ ).

In Fig.1 we have shown the region allowed by the Kamiokande data in the plane of the parameters  $B_{\nu_e;\nu_e}$  and  $\Delta m^2$ . We have also shown the forbidden regions (on the right of the corresponding curves) that were found from the analysis of the data from the Bugey [35] and Krasnoyarsk [36] reactor experiments and the region of sensitivity of the future CHOOZ [24] reactor experiment. It is seen from Fig.1 that a large part of the region in the  $B_{\nu_e;\nu_e}$ – $\Delta m^2$  plane that is allowed by the Kamiokande atmospheric neutrino data will be investigated by future long-baseline reactor experiments.

In Fig.2 we have shown the region allowed by the Kamiokande data in the  $B_{\nu_\mu;\nu_\mu}$ – $\Delta m^2$  plane. As can be seen from Fig.2, only large values of  $B_{\nu_\mu;\nu_\mu}$  ( $B_{\nu_\mu;\nu_\mu} \gtrsim 0.5$ ) are allowed by the results of this experiment. The regions of sensitivity of the future BNL E889 [26], MINOS [27] and KEK–Super-Kamiokande [25] long-baseline experiments are also shown. It is seen from this figure that a large part of the region of the  $B_{\nu_\mu;\nu_\mu}$ – $\Delta m^2$  plane, including the Kamiokande-allowed region, will be investigated in future long-baseline accelerator disappearance experiments.

The Kamiokande-allowed region in the plane of the parameters  $A_{\nu_\mu;\nu_e}$  and  $\Delta m^2$  is shown in Fig.3. In this figure we have also shown the regions that are forbidden by the results of the Bugey and Krasnoyarsk reactor experiments and the regions of sensitivity of the future KEK-SK, MINOS and ICARUS [28] long-baseline experiments (we have used the inequality  $A_{\nu_\mu;\nu_e} \leq B_{\nu_e;\nu_e}$ ). Finally, in Fig.4 we present the results of our calculations of the allowed region in the plane of the parameters  $A_{\nu_\mu;\nu_\tau}$  and  $\Delta m^2$ . The region limited by the solid lines is allowed by the Kamiokande data alone. A large part of this region is excluded by the results of reactor experiments. In fact, for relatively small values of the amplitude  $A_{\nu_\mu;\nu_\tau}$ , the fit of the Kamiokande data requires large values of the amplitude  $A_{\nu_\mu;\nu_e}$ , which, due to inequality  $A_{\nu_\mu;\nu_e} \leq B_{\nu_e;\nu_e}$ , can be in contradiction with the results of reactor experiments. The region in the  $A_{\nu_\mu;\nu_\tau}$ – $\Delta m^2$  plane that is allowed by the Kamiokande data and by the results of the Bugey and Krasnoyarsk reactor experiments lies on the right of the dotted line in Fig.4. As can be seen from Fig.4, the Kamiokande atmospheric neutrino data allow large values of the amplitude of  $\nu_\mu \rightleftharpoons \nu_\tau$  oscillations and the values of the parameter  $\Delta m^2$  in the range

$$8 \times 10^{-3} \text{ eV}^2 \lesssim \Delta m^2 \lesssim 8 \times 10^{-2} \text{ eV}^2. \quad (4.1)$$

For a neutrino energy  $E \simeq 15 \text{ GeV}$ , the range (4.1) corresponds to the following range of possible values of the oscillation length:

$$450 \text{ Km} \lesssim L_{\text{osc}} \lesssim 4500 \text{ Km}. \quad (4.2)$$

Therefore, a large effect of  $\nu_\mu \rightarrow \nu_\tau$  oscillations could be observed with the long-baseline neutrino oscillation experiments now under preparation at CERN and FNAL with detectors

placed in the Gran Sasso Laboratory and in the Soudan Mine, at a distance of about 730 Km from the corresponding neutrino source. The best fit of the Kamiokande data corresponds to  $L_{\text{osc}} \simeq 1400$  Km. Thus, a large fraction of the charged-current events in long-baseline experiments could be events in which  $\tau$  is produced.

In Fig.4 we have also shown the region in the plane of the parameters  $A_{\nu_\mu, \nu_\tau} - \Delta m^2$  that is forbidden by the data of the CDHS experiment [37] in which  $\nu_\mu$  disappearance was searched for. It can be seen that this forbidden region is far away from the region allowed by the Kamiokande data.

Up to now we have discussed the results of the analysis of the data of the Kamiokande experiment. It is interesting to see what happens to the quality of the fit as well as to the allowed regions if we make a combined analysis of the Kamiokande data, which indicate neutrino oscillation effects, and the Frejus data, which are not in contradiction with the absence of neutrino oscillations.

We have found that the Kamiokande and Frejus data can simultaneously be explained in the framework of our three parameters model with mixing among three neutrinos. For 18 degrees of freedom we obtained  $\chi^2_{\text{min}} = 22$  at  $\Delta m^2 = 1.4 \times 10^{-2} \text{ eV}^2$ ,  $|U_{e3}|^2 = 0.06$  and  $|U_{\mu 3}|^2 = 0.23$  (with a CL of 22%). The results of the combined fit are presented in Figs.5–8. In each of these figures we have shown the regions in the plane of two parameters which is allowed both by Kamiokande and Frejus data at 90% CL. We have also shown the regions forbidden by the data of the reactor and accelerator experiments and the regions of sensitivity of the future long-baseline experiments.

In conclusion, we would like to make the following remark: in order to accommodate the solar neutrino data it is necessary to require that the parameter  $|U_{e3}|$  is not too large. In fact, the survival probability of solar neutrinos is given by [38]

$$P_{\nu_e \rightarrow \nu_e}(E) = (1 - |U_{e3}|^2)^2 P_{\nu_e \rightarrow \nu_e}^{(1,2)}(E) + |U_{e3}|^4 , \quad (4.3)$$

where  $P_{\nu_e \rightarrow \nu_e}^{(1,2)}(E)$  is the survival probability due to the mixing between the first and the second generations. From Eq.(4.3) it is clear that  $P_{\nu_e \rightarrow \nu_e}(E) \geq |U_{e3}|^4$  for all values of  $E$ . On the other hand, from a model independent analysis of the solar neutrino data (see Ref. [39]) it follows that for  ${}^7\text{Be}$  neutrinos  $P_{\nu_e \rightarrow \nu_e} \lesssim 0.5$ . Therefore, large values of  $|U_{e3}|$  are excluded by the solar neutrino data. We have first performed the analysis of the experimental data without any constraint on the value of  $|U_{e3}|$ . Then the analysis was repeated with the constraints  $|U_{e3}|^2 \leq 0.7$  and  $|U_{e3}|^2 \leq 0.5$ . However, the inclusion of these constraints did not induce any modification of the allowed regions of the parameters (this is due to the fact that all the allowed values of the oscillation amplitudes can be obtained with  $|U_{e3}|^2 \leq 0.5$ ). Therefore, all the allowed regions shown in the figures are consistent with the solar neutrino data.

## V. CONCLUSIONS

A wide range of reactor and accelerator long-baseline neutrino experiments which will investigate different channels of neutrino oscillations in the range  $\Delta m^2 \simeq 10^{-3} - 10^{-2} \text{ eV}^2$  and a broad range of oscillation amplitudes is at present under development at Fermilab, CERN

and other laboratories. Taking into account these new possibilities for the investigation of neutrino mixing, we have presented here the results of an analysis of the data of the underground experiments on the detection of the atmospheric neutrinos, in some of which (Kamiokande, IMB, Soudan 2) positive indications in favor of neutrino oscillations were found.

The analysis has been carried out by using the framework of a model with mixing of three massive neutrino fields which permit simultaneous oscillations among all active neutrinos. We have assumed that there are two scales of neutrino mass squared difference which can accommodate the solar neutrino problem (at a scale of about  $10^{-5}$  eV $^2$ ) and the atmospheric neutrino anomaly (at a scale of about  $10^{-2}$  eV $^2$ ). In this model all oscillation channels for atmospheric and terrestrial neutrinos are characterized by the same oscillation length  $L_{\text{osc}} = 4\pi p/\Delta m^2$  and the oscillation amplitudes in different channels are determined by the two parameters  $|U_{e3}|^2$  and  $|U_{\mu 3}|^2$ . Due to the unitarity of the mixing matrix, different oscillation amplitudes are connected by the relations (2.9)–(2.11).

The results of the analysis of the atmospheric neutrino data are presented in the form of plots in the plane of the two parameters oscillation amplitude and  $\Delta m^2$ . In our analysis we have considered the following channels:  $\nu_\mu \rightleftharpoons \nu_x$ ,  $\nu_e \rightleftharpoons \nu_x$ ,  $\nu_\mu \rightleftharpoons \nu_e$  and  $\nu_\mu \rightleftharpoons \nu_\tau$ . In the figures we have also presented the limits that were obtained in reactor and accelerator experiments searching for neutrino oscillations as well as the regions in different oscillation channels that will be investigated in future long-baseline experiments. The results of the analysis of the Kamiokande data are shown in Figs.1–4 and those of the combined analysis of the Kamiokande and Frejus data are shown in Figs.5–8.

## ACKNOWLEDGMENTS

It is a pleasure to thank A. Bottino for useful discussions. C.W.K. would like to thank the Sezione di Torino of INFN for its hospitality during the completion of this work. This work was supported in part by the National Science Foundation.

## REFERENCES

- [1] R. Davis Jr., *Proc. of the 6<sup>th</sup> International Workshop on Neutrino Telescopes*, Venezia, March 1994.
- [2] K. S. Hirata et al., Phys. Rev. Lett. **65**, 1297 (1990); Phys. Rev. D **44**, 2241 (1991); Y. Suzuki, *Proc. of the 6<sup>th</sup> International Workshop on Neutrino Telescopes*, Venezia, March 1994.
- [3] GALLEX Coll., Phys. Lett. B **285**, 376 (1992); Phys. Lett. B **314**, 445 (1993); Phys. Lett. B **327**, 377 (1994); Phys. Lett. B **342**, 440 (1995).
- [4] J.N. Abdurashitov et al., Phys. Lett. B **328**, 234 (1994); *Proc. of the 27<sup>th</sup> Int. Conf. on High Energy Physics*, Glasgow, July 1994.
- [5] S.P. Mikheyev and A.Yu. Smirnov, Yad. Fiz. **42**, 1441 (1985) [Sov. J. Nucl. Phys. **42**, 913 (1985)]; Il Nuovo Cimento C **9**, 17 (1986); L. Wolfenstein, Phys. Rev. D **17**, 2369 (1978); Phys. Rev. D **20**, 2634 (1979).
- [6] G. Barr, T.K. Gaisser and T. Stanev, Phys. Rev. D **39**, 3532 (1989); G. Barr, T.K. Gaisser, S. Tilav and D. Lipari, Phys. Lett. B **214**, 147 (1988); W. Frati, T.K. Gaisser, A.K. Mann and T. Stanev, Phys. Rev. D **48**, 1140 (1993); T.K. Gaisser, Nucl. Phys. B (Proc. Suppl.) **35**, 209 (1994).
- [7] E.V. Bugaev and V.A. Naumov, Yad. Fiz. **45**, 1380 (1987) [Sov. J. Nucl. Phys. **45**, 857 (1987)]; Phys. Lett. B **232**, 391 (1989).
- [8] M. Honda et al., Phys. Lett. B **248**, 193 (1990); ICRR-336-95-2, March 1995 (hep-ph@xxx.lanl.gov/9503439).
- [9] D.H. Perkins, Astropart. Phys. **2**, 249 (1994).
- [10] K.S. Hirata, Phys. Lett. B **205**, 416 (1988).
- [11] K.S. Hirata et al., Phys. Lett. B **280**, 146 (1992).
- [12] Y. Fukuda et al., Phys. Lett. B **335**, 237 (1994).
- [13] D. Casper et al., Phys. Rev. Lett. **66**, 2561 (1991); R. Becker-Szendy et al., Phys. Rev. D **46**, 3720 (1992); R. Becker-Szendy et al., Nucl. Phys. B (Proc. Suppl.) **38**, 331 (1995).
- [14] T. Kafka, Nucl. Phys. B (Proc. Suppl.) **35**, 427 (1994); M. Goodman, Nucl. Phys. B (Proc. Suppl.) **38**, 337 (1995).
- [15] C. Berger et al., Phys. Lett. B **227**, 489 (1989).
- [16] C. Berger et al., Phys. Lett. B **245**, 305 (1990).
- [17] K. Daum et al., WUB 95-03, Feb. 1995, to be published in Z. Phys. C.
- [18] M. Aglietta et al., Europhys. Lett. **8**, 611 (1989); Europhys. Lett. **15**, 559 (1991).
- [19] M. Mori et al., Phys. Lett. B **270**, 89 (1991).
- [20] R. Becker-Szendy et al., Phys. Rev. Lett. **69**, 1010 (1992).
- [21] M.M. Boliev et al., *Proc. of the 3<sup>th</sup> International Workshop on Neutrino Telescopes*, Venezia, March 1991.
- [22] D. Michael for the MACRO Coll., Talk presented at the 1994 *Snowmass Summer Study*, July 1994.
- [23] D. Crane and M. Goodman, NuMI note NUMI-L-44, June 1994; R. Rameika, NUMI-72, April 1995.
- [24] R.I. Steinberg, *Proc. of the 5<sup>th</sup> International Workshop on Neutrino Telescopes*, Venezia, March 1993.

- [25] K. Nishikawa, INS-Rep-924, April 1992; C.B. Bratton et al., *Proposal to Participate in the Super-Kamiokande Project*, Dec. 1992.
- [26] A.K. Mann et al., BNL-PROPOSAL-889, Jan 1993.
- [27] MINOS Coll., NuMI note NUMI-L-63, February 1995; NUMI-L-79, April 1995.
- [28] ICARUS Coll., Gran Sasso Lab. preprint LNGS-94/99-I, May 1994.
- [29] G.L. Fogli, E. Lisi and D. Montanino, Phys. Rev. D **49**, 3626 (1994); CERN-TH-7491-94, November 1994.
- [30] M. Gell-Mann, P. Ramond, and R. Slansky, in *Supergravity*, ed. F. van Nieuwenhuizen and D. Freedman, (North Holland, Amsterdam, 1979) p. 315; T. Yanagida, *Proc. of the Workshop on Unified Theory and the Baryon Number of the Universe*, KEK, Japan, 1979; S. Weinberg, Phys. Rev. Lett. **43**, 1566 (1979).
- [31] S.M. Bilenky and B. Pontecorvo, Phys. Rep. **41**, 225 (1978); S.M. Bilenky and S.T. Petcov, Rev. Mod. Phys. **59**, 671 (1987).
- [32] C.W. Kim and A. Pevsner, *Neutrinos in Physics and Astrophysics*, Contemporary Concepts in Physics, Vol. 8, (Harwood Academic Press, Chur, Switzerland, 1993).
- [33] A. De Rujula et al., Nucl. Phys. B **168**, 54 (1980); V. Barger and K. Whisnant, Phys. Lett. B **209**, 365 (1988); S.M. Bilenky, M. Fabbrichesi and S.T. Petcov, Phys. Lett. B **276**, 223 (1992).
- [34] E.D. Carlson, Phys. Rev. D **34**, 1454 (1986); G. Auriemma et al., Phys. Rev. D **37**, 665 (1988); E. Akhmedov, P. Lipari and M. Lusignoli, Phys. Lett. B **300**, 128 (1993).
- [35] B. Achkar et al., Nucl. Phys. B **434**, 503 (1995).
- [36] G.S. Vidyakin et al., JETP Lett. **59**, 390 (1994).
- [37] F. Dydak et al., Phys. Lett. B **134**, 281 (1984).
- [38] T.K. Kuo and J. Pantaleone, Phys. Rev. Lett. **57**, 1805 (1986); X. Shi and D.N. Schramm, Phys. Lett. B **283**, 305 (1992).
- [39] J.N. Bahcall, Phys. Lett. B **338**, 276 (1994).

## FIGURES

FIG. 1. Region of the parameters  $B_{\nu_e;\nu_e}$  and  $\Delta m^2$  allowed at 90% CL by the Kamiokande data (within the two solid lines). The regions on the right of the dashed and dotted lines are forbidden by the results of the Bugey and Krasnoyarsk experiments, respectively. The dash-dotted line indicates the sensitivity of the future long-baseline CHOOZ experiment.

FIG. 2. Region of the parameters  $B_{\nu_\mu;\nu_\mu}$  and  $\Delta m^2$  allowed at 90% CL by the Kamiokande data (within the solid line). The region on the right of the short-dashed line is forbidden by the results of the CDHS experiment. The dash-dotted, dash-dot-dotted and long-dashed lines indicate the sensitivity of the future long-baseline BNL E889, MINOS and KEK–Super-Kamiokande experiments, respectively.

FIG. 3. Region of the parameters  $A_{\nu_\mu;\nu_e}$  and  $\Delta m^2$  allowed at 90% CL by the Kamiokande data (within the two solid lines). The regions on the right of the dashed and dotted lines are forbidden by the results of the Bugey and Krasnoyarsk experiments, respectively. The dash-dotted, dash-dot-dotted and long-dashed lines indicate the sensitivity of the future long-baseline ICARUS, MINOS and KEK–Super-Kamiokande experiments, respectively.

FIG. 4. Region of the parameters  $A_{\nu_\mu;\nu_\tau}$  and  $\Delta m^2$  allowed at 90% CL by the Kamiokande data (within the two solid lines). The region on the left of the dotted line is excluded by the results of the Krasnoyarsk and Bugey reactor experiments. The dash-dotted and dash-dot-dotted lines indicate the sensitivity of the future long-baseline ICARUS and MINOS experiments, respectively.

FIG. 5. Region of the parameters  $B_{\nu_e;\nu_e}$  and  $\Delta m^2$  allowed at 90% CL by the Kamiokande and Frejus data (within the solid line). The regions on the right of the dashed and dotted lines are forbidden by the results of the Bugey and Krasnoyarsk experiments, respectively. The dash-dotted line indicates the sensitivity of the future long-baseline CHOOZ experiment.

FIG. 6. Region of the parameters  $B_{\nu_\mu;\nu_\mu}$  and  $\Delta m^2$  allowed at 90% CL by the Kamiokande and Frejus data (within the solid line). The region on the right of the short-dashed line is forbidden by the results of the CDHS experiment. The dash-dotted, dash-dot-dotted and long-dashed lines indicate the sensitivity of the future long-baseline BNL E889, MINOS and KEK–Super-Kamiokande experiments, respectively.

FIG. 7. Region of the parameters  $A_{\nu_\mu;\nu_e}$  and  $\Delta m^2$  allowed at 90% CL by the Kamiokande and Frejus data (within the solid line). The regions on the right of the dashed and dotted lines are forbidden by the results of the Bugey and Krasnoyarsk experiments, respectively. The dash-dotted, dash-dot-dotted and long-dashed lines indicate the sensitivity of the future long-baseline ICARUS, MINOS and KEK–Super-Kamiokande experiments, respectively.

FIG. 8. Region of the parameters  $A_{\nu_\mu;\nu_\tau}$  and  $\Delta m^2$  allowed at 90% CL by the Kamiokande and Frejus data (within the solid line). The region on the left of the dotted line is excluded by the results of the Krasnoyarsk and Bugey reactor experiments. The dash-dotted and dash-dot-dotted lines indicate the sensitivity of the future long-baseline ICARUS and MINOS experiments, respectively.

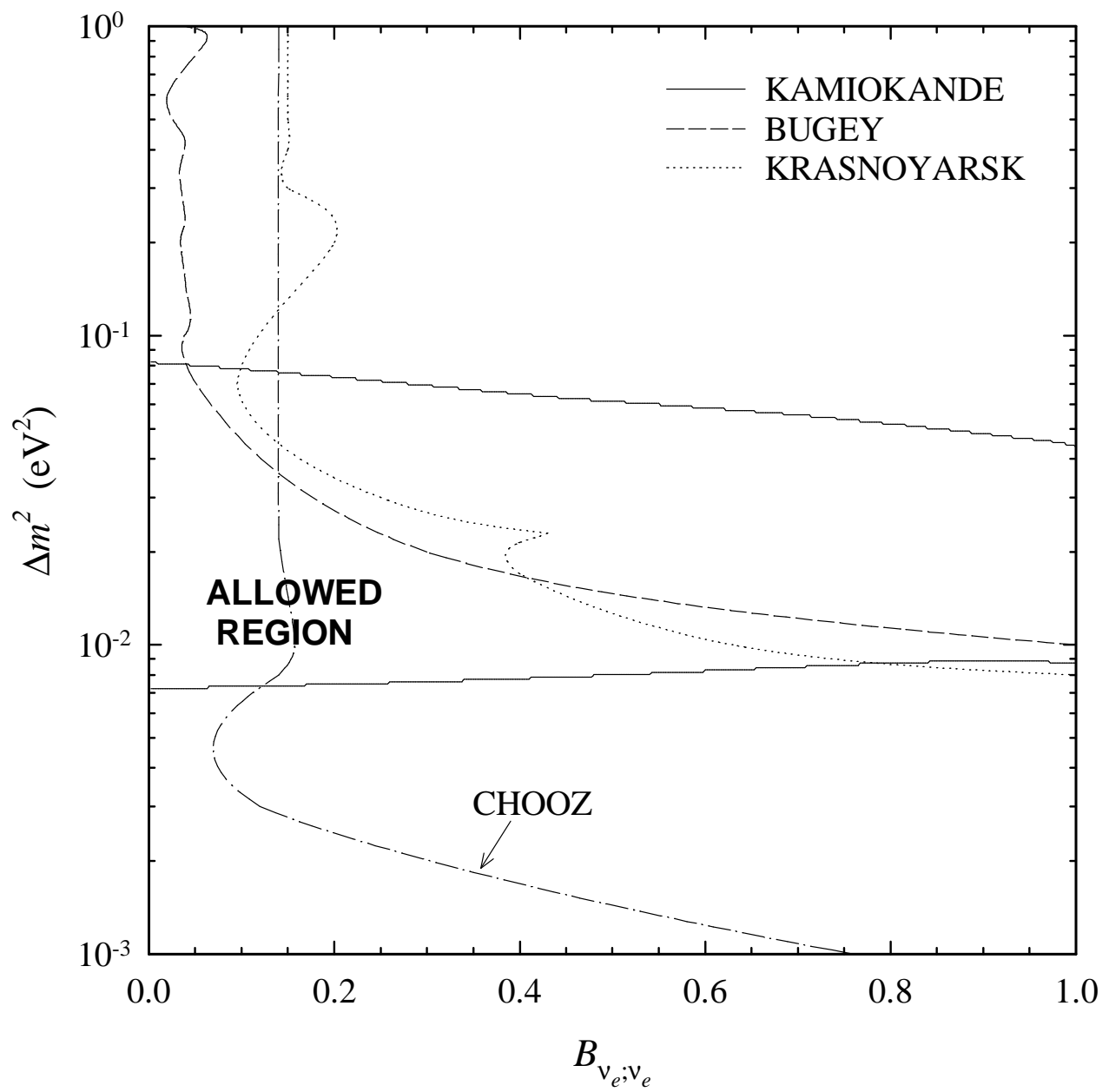


Figure 1

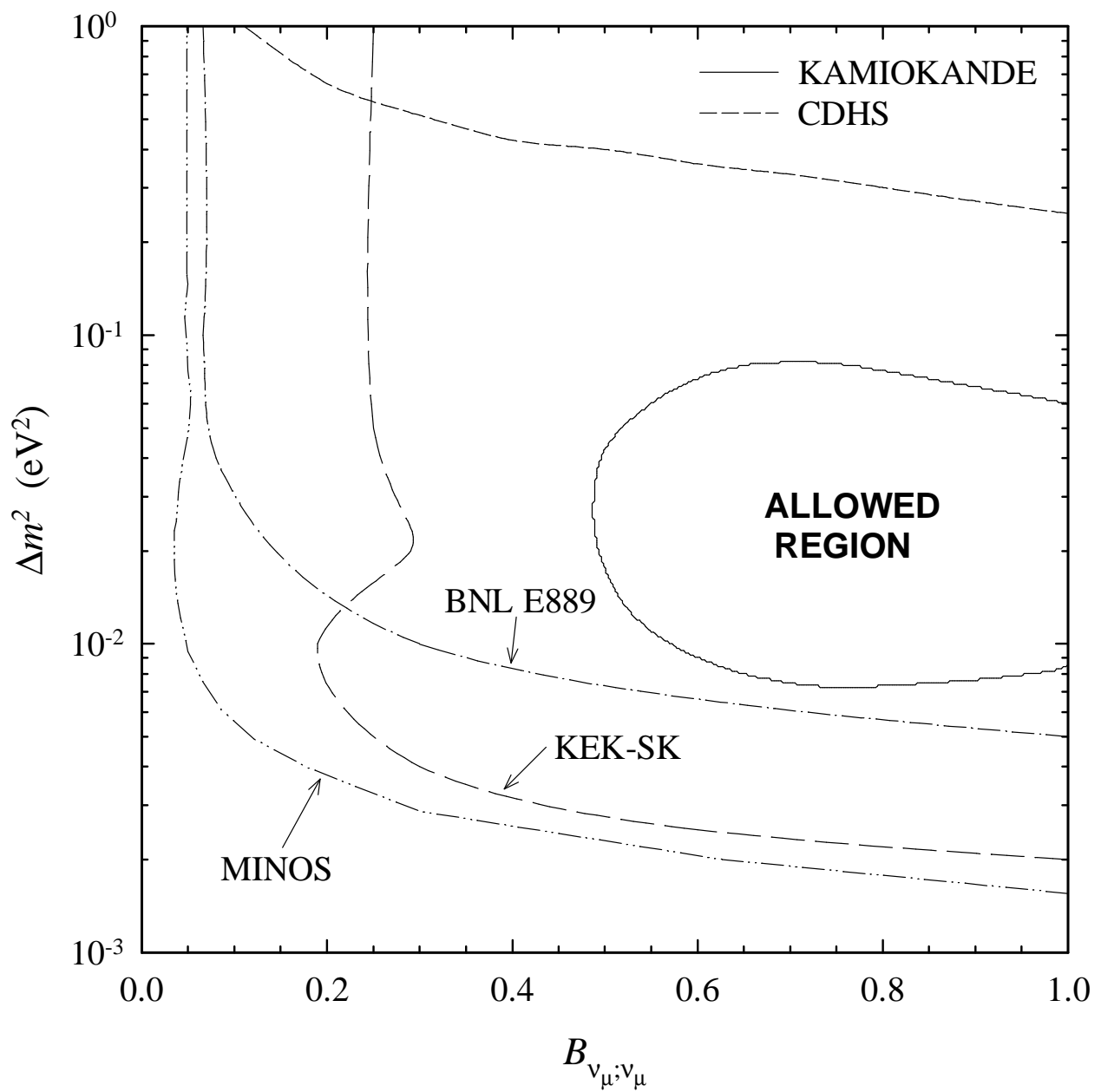


Figure 2

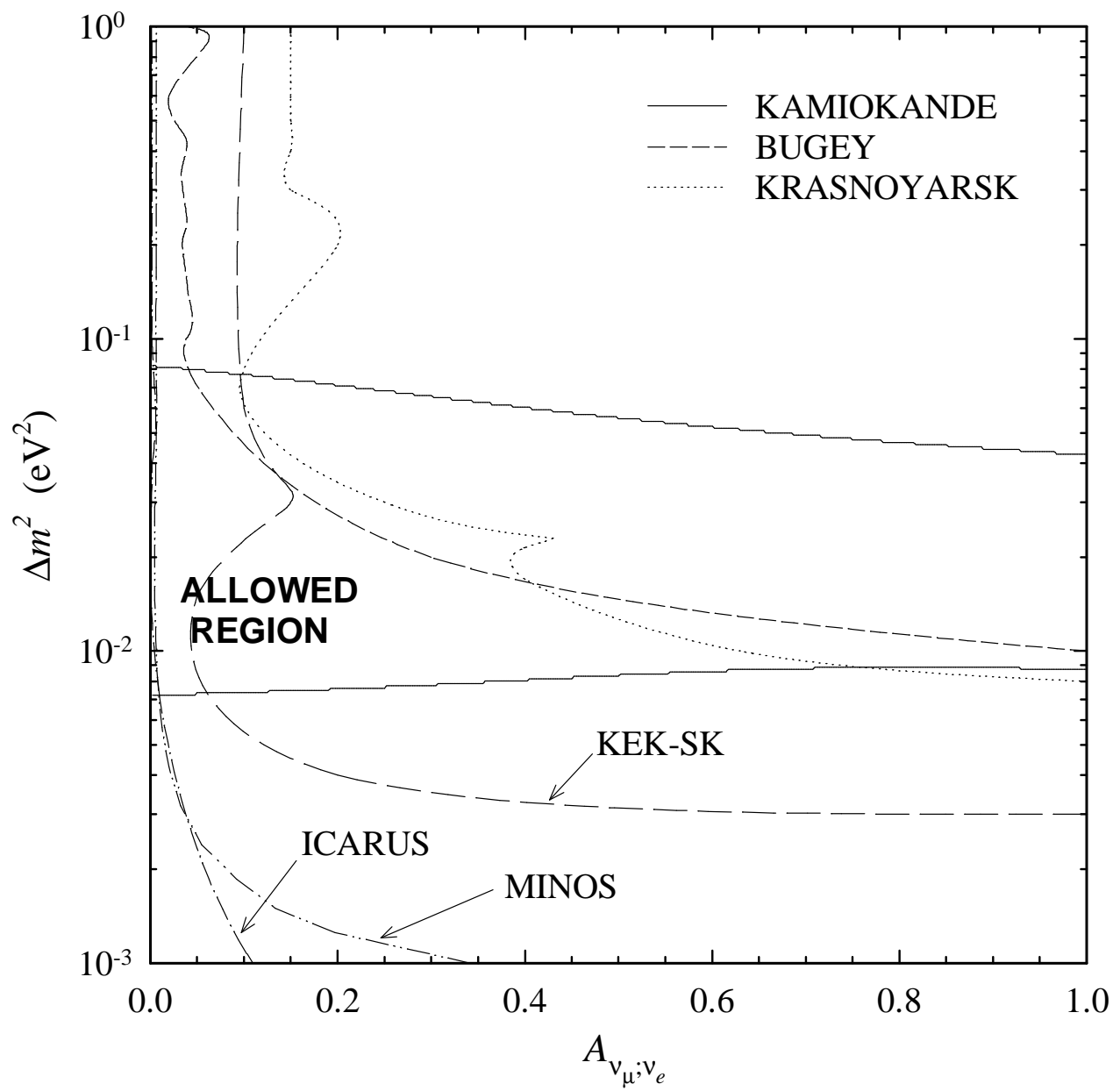


Figure 3

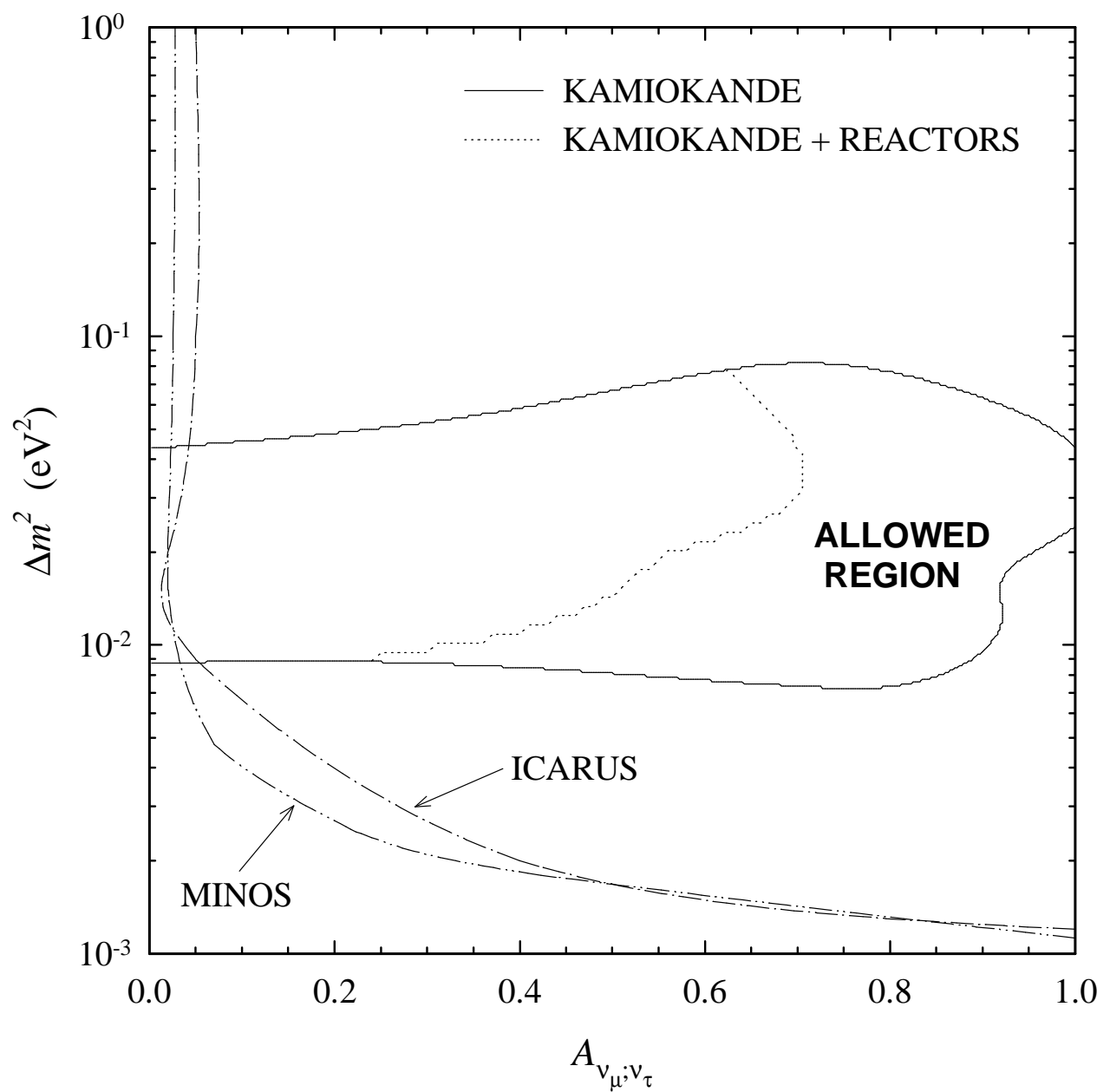


Figure 4

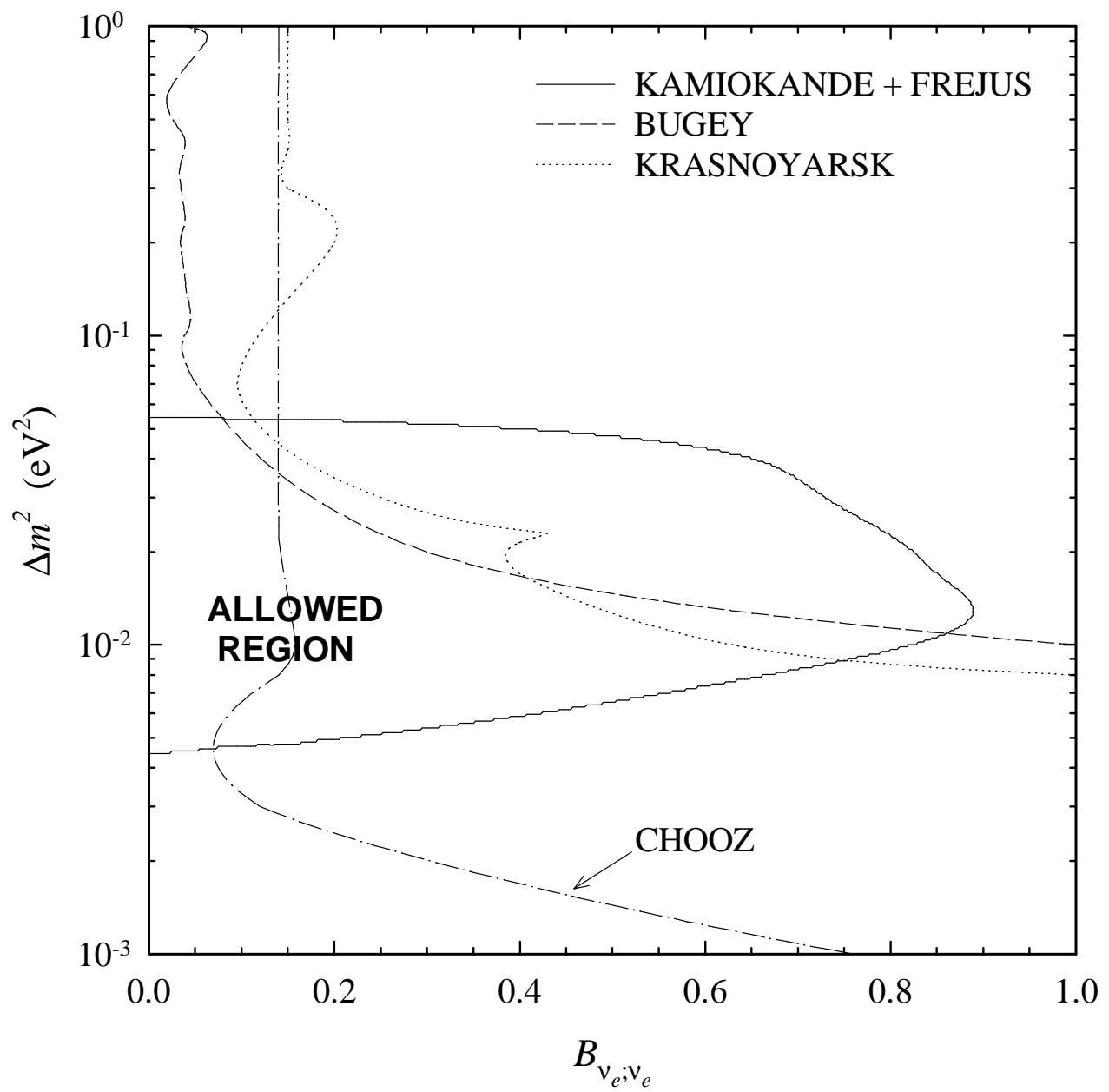


Figure 5

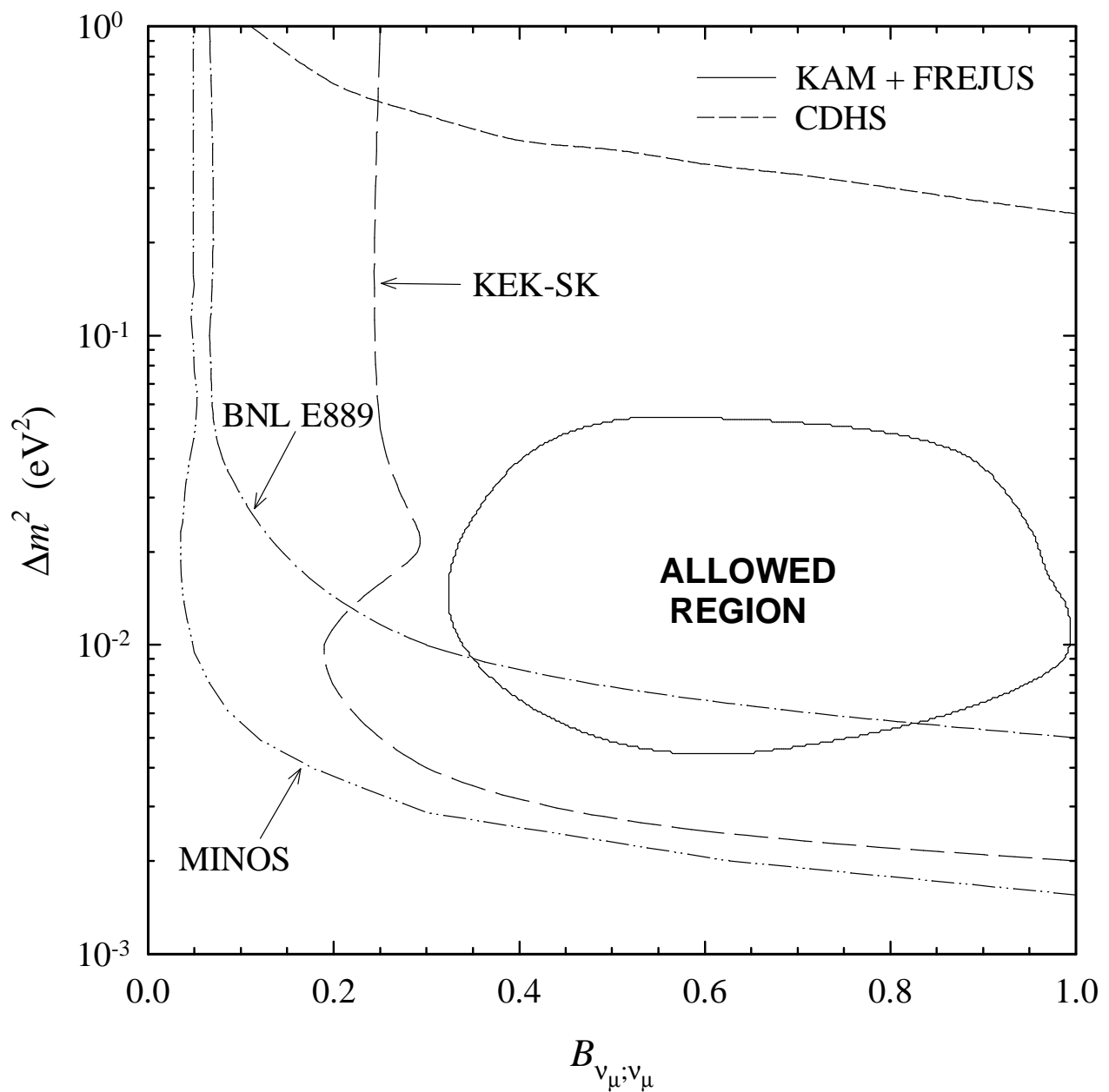


Figure 6

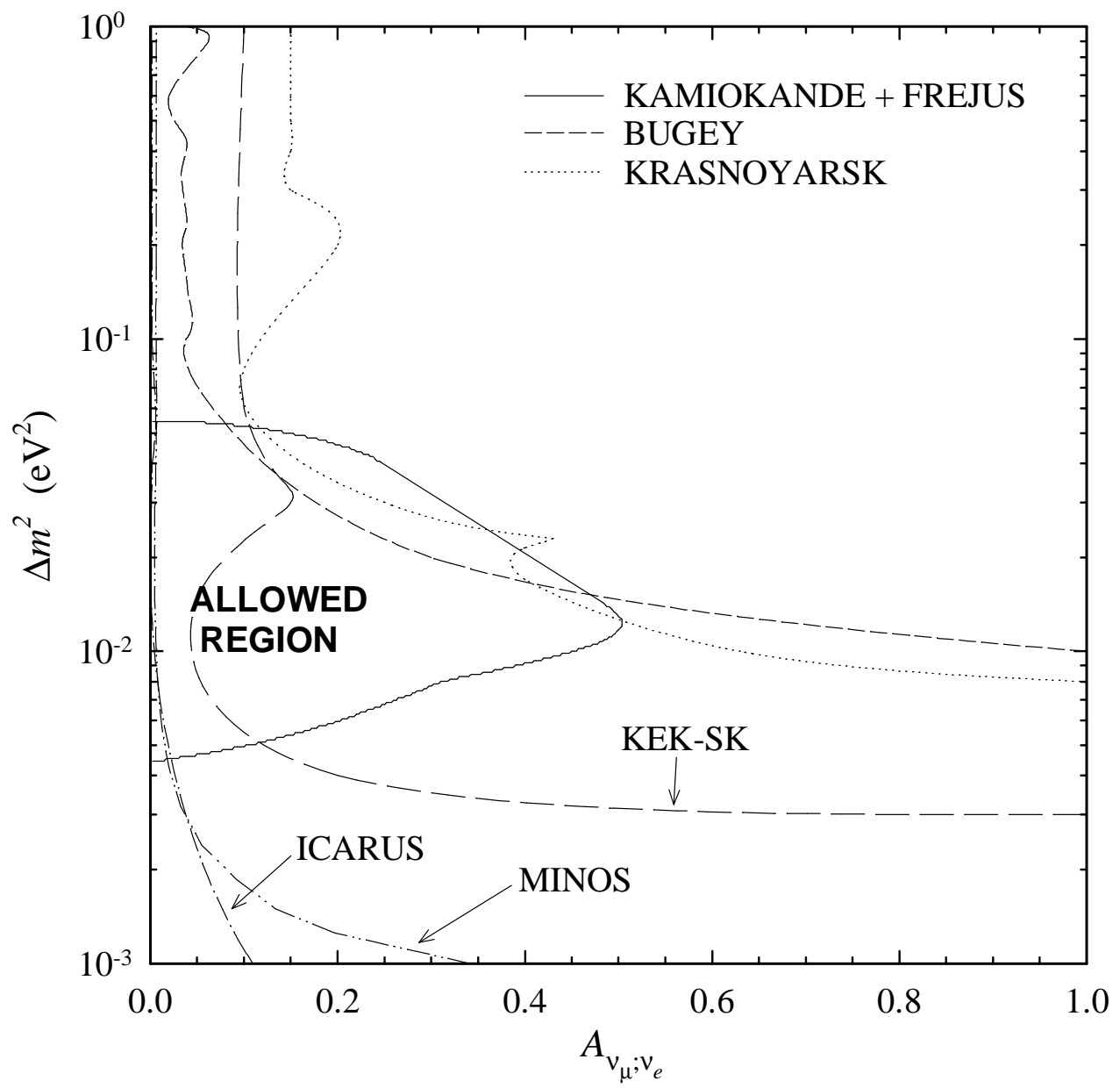


Figure 7

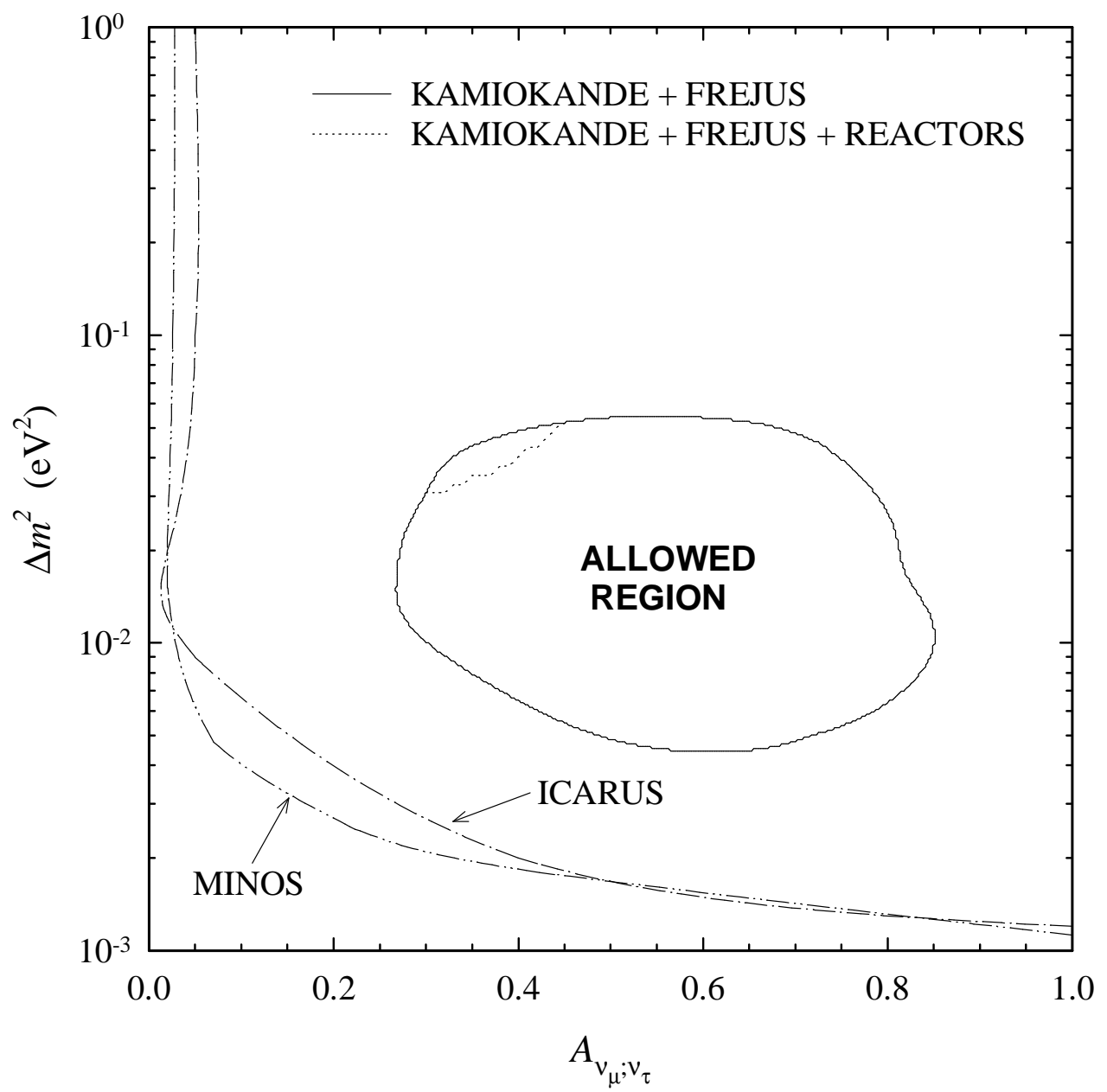


Figure 8